



# Theoretical Modeling and Optimization of Porous Coating for Hypersonic Laminar Flow Control

R. Zhao\*

Beijing Institute of Technology, 100081 Beijing, People's Republic of China  
and

T. Liu,<sup>†</sup> C. Y. Wen,<sup>‡</sup> J. Zhu,<sup>§</sup> and L. Cheng<sup>¶</sup>

Hong Kong Polytechnic University, Kowloon, People's Republic of China

DOI: 10.2514/1.J057272

A theoretical model is developed to describe the acoustic characteristics of plane ultrasonic acoustic waves impinging on a porous coating, namely, a rigid surface periodically corrugated with subwavelength grooves (two-dimensional cavities). The proposed model takes into account the high-order diffracted modes, and therefore incorporates mutual coupling among neighboring cavities. The model predicts a reflection frequency consistent with the numerical results and reproduces a coupling mode induced by interactions between waves scattered from adjacent cavities. With this model, the cavity geometry parameters are optimized to achieve the minimum reflection coefficient. The result shows that the Mack second mode is strongly suppressed and that the maximum fluctuating pressure decreases by about 88% upon using the optimized porous coating in a Mach 6 flat-plate flow.

## Nomenclature

$A$	=	porous layer admittance
$A_r$	=	cavity aspect ratio; $2b/H$
$b$	=	cavity half-width
$f_{acs}$	=	normalized acoustic frequency; $fH/a_w$
$H$	=	thickness of porous layer
$R$	=	reflection coefficient
$T$	=	temperature
$t$	=	time
$x, y$	=	streamwise and normal directions
$\rho$	=	density
$\phi$	=	porosity, $2b/s$
$\omega$	=	angular frequency

## Subscripts

$c$	=	waves in the cavity
$i$	=	incident waves
$r$	=	diffracted waves
$w$	=	parameters at the wall
$\infty$	=	freestream

## I. Introduction

VARIOUS techniques have been developed to prevent or delay hypersonic boundary-layer transition [1–3]. One of the most promising control technologies is the passive porous coating concept

Received 7 March 2018; revision received 9 May 2018; accepted for publication 19 May 2018; published online 16 July 2018. Copyright © 2018 by the American Institute of Aeronautics and Astronautics, Inc. All rights reserved. All requests for copying and permission to reprint should be submitted to CCC at [www.copyright.com](http://www.copyright.com); employ the ISSN 0001-1452 (print) or 1533-385X (online) to initiate your request. See also AIAA Rights and Permissions [www.aiaa.org/randp](http://www.aiaa.org/randp).

\*Assistant Professor, School of Aerospace Engineering and Research Assistant, Department of Mechanical Engineering; also Hong Kong Polytechnic University, Kowloon, Hong Kong Special Administrative Region.

<sup>†</sup>Ph.D. Candidate, Department of Mechanical Engineering, Hong Kong Special Administrative Region.

<sup>‡</sup>Professor, Department of Mechanical Engineering, Hong Kong Special Administrative Region; [cywen@polyu.edu.hk](mailto:cywen@polyu.edu.hk). Associate Fellow AIAA (Corresponding Author).

<sup>§</sup>Assistant Professor, Department of Mechanical Engineering, Hong Kong Special Administrative Region.

<sup>¶</sup>Professor, Department of Mechanical Engineering, Hong Kong Special Administrative Region.

proposed by Fedorov et al. [4] because of its minimal effect on mean flow and the effective suppression of the most unstable boundary-layer instability: namely, the Mack second mode [5–7]. The effect of a porous coating on the hypersonic boundary layer can be either theoretically interpreted by the porous boundary condition of vertical velocity at the wall ( $v'_w = Ap'_w$  [4,8]) or numerically investigated by directly resolving the flowfield within the microstructures [9–11]. The first method is more convenient when we focus on the influences of the geometry parameters of microstructures without the need to modify the computational mesh. The admittance  $A$  is a complex quantity that depends on the properties of the wall material, porosity parameters, mean flow characteristics at the wall surface, and flow-perturbation parameters such as wave frequency and wavelength. The equation for admittance is derived by applying the theory of sound wave propagation in a thin, long tube [12]. Although this theoretical model, hereinafter called Fedorov's model, has been widely applied (see recent works in Refs. [13–15]), it does not take into account the high-order diffracted waves, and thus underestimates the coupling among adjacent cavities as well as their contribution to the overall admittance [16–18]. This simplification is considered to be responsible for the low-frequency shift of the reflection curves [14,19]. The design of this porous coating device and its integration with thermal protection systems require the development of accurate models of the effect of the porous coating. In particular, further optimization requires frequency matching between the most amplified Mack second-mode instability wave and the minimum reflection property of microstructures.

In the present study, we improve the porous coating model by considering high-order diffracted waves when the acoustic disturbance penetrates the porous surface. In this way, the scattering and coupling effect is more carefully taken into account. Based on the proposed model, a straightforward optimization procedure is introduced to maximize the absorption of the porous layer.

## II. Theoretical Model and Optimization

As shown in Fig. 1, the porous surface is a rigid surface periodically corrugated with subwavelength grooves (two-dimensional cavities) being infinitely extended in the  $x$  direction. The background medium is assumed to have uniform and constant density  $\rho_w$  and sound speed  $c_w$ . The subscript  $w$  denotes the local physical quantity at the wall. The half-width and depth of the cavities are  $b$  and  $H$ , respectively, with the unit-cell period being  $s$ . The porosity and aspect ratio are  $\phi = 2b/s$  and  $Ar = 2b/H$ , respectively. These definitions are in accordance with previous research [14,19].

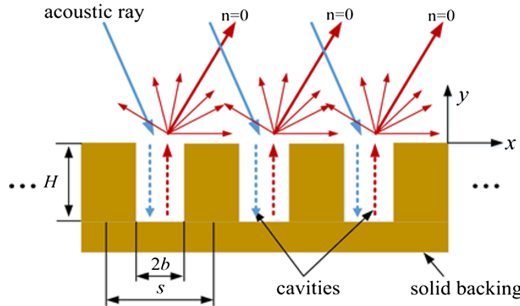


**Fig. 1** Schematic drawing of reflection of acoustic waves from equally spaced two-dimensional cavities.

The acoustic field and the surface admittance of such textured surface can be analytically obtained in the plane wave expansion method [16–18]. An obliquely incident plane acoustic wave can be written as (the time dependence  $e^{-j\omega t}$  is omitted for simplicity)

$$p_i = e^{jk_x x} e^{-jk_y y},$$

$$v_{y,i} = \frac{1}{j\omega\rho_w} \frac{\partial p_i}{\partial y} = -\frac{k_y}{\rho_w\omega} e^{jk_x x} e^{-jk_y y} \quad (1)$$

where  $p_i$  is the incident pressure,  $v_{y,i}$  is the  $y$  component of the particle velocity, and  $j = \sqrt{-1}$ . Note that  $k_x$  is the parallel momentum and  $k_y = (k_0^2 - k_x^2)^{1/2}$  is the perpendicular momentum, in which  $k_0 = \omega/c_w$  is the wave number with  $\omega$  being the angular frequency. The reflected pressure field  $p_r^n$  and  $y$ -component particle velocity  $v_{y,r}^n$  of the  $n$ th-order diffracted wave are expressed as

$$p_r^{(n)} = R_n e^{jk_x^{(n)} x} e^{jk_y^{(n)} y},$$

$$v_{y,r}^{(n)} = \frac{k_y^{(n)}}{\rho_w\omega} R_n e^{jk_x^{(n)} x} e^{jk_y^{(n)} y} \quad (2)$$

where  $k_x^{(n)} = k_x + 2\pi n/s$ ,  $k_y^{(n)} = [k_0^2 - (k_x^{(n)})^2]^{1/2}$ ,  $n \in \mathbf{Z}$ , and  $R_n$  is the reflection coefficient of the  $n$ th-order diffraction. Inside the cavities, the fundamental wave mode dominates for a long wavelength limit ( $2b \ll \lambda_{acs}$ , where  $\lambda_{acs}$  is the wavelength of the incident acoustic wave), and the sound pressure and particle velocity within the cavity are denoted as

$$p_c = C_1 e^{jk_c y} + C_2 e^{-jk_c y},$$

$$v_{y,c} = \frac{k_c}{\tilde{\rho}\omega} (C_1 e^{jk_c y} - C_2 e^{-jk_c y}) \quad (3)$$

where the dynamic density  $\tilde{\rho}$ , compressibility  $\tilde{C}$ , and wave number  $k_c$  are complex and frequency-dependent quantities owing to the thermal and viscous boundary layers inside the narrow cavity:

$$\tilde{\rho} = \rho_w / \Psi_v, \quad \tilde{C} = \frac{\gamma - (\gamma - 1)\Psi_t}{\rho_w c_w^2},$$

$$k_c^2 = \omega^2 \tilde{\rho} \tilde{C} = k_0^2 \frac{\gamma - (\gamma - 1)\Psi_t}{\Psi_v} \quad (4)$$

Here,  $\Psi_i = 1 - \tan(k_i b)/k_i b$  with

$$k_i^2 = \begin{cases} k_v^2 = j\omega \frac{\rho_w}{\mu} & \text{viscous wave number} \\ k_t^2 = j\omega \frac{\rho_w C_p}{\kappa} & \text{thermal wave number} \end{cases}$$

The subscript  $i$  is either  $v$  or  $t$  to denote the effects of viscous or thermal boundary layers, respectively. In the aforementioned equations,  $\kappa$  is thermal conductivity,  $\mu$  is viscosity, and  $\gamma = C_p/C_v$  is the ratio of the specific heat at constant pressure  $C_p$  to specific heat at constant volume  $C_v$ .

The bottom of the cavity is rigid ( $v_{y,c}|_{y=-H} = 0$ ); thus,  $C_1 = C_2 e^{2jk_c H} \equiv C e^{2jk_c H}$ . At the interface between the upper half-space and the cavity opening mouth, the sound pressure should be continuous:

$$\frac{1}{2b} \int_{x=-b}^{x=b} \left( e^{jk_x x} + \sum_{n=-\infty}^{+\infty} R_n e^{jk_x^{(n)} x} \right) dx = C(1 + e^{2jk_c H}) \quad (5)$$

Equation (5) is then deduced as

$$\sum_{n=-\infty}^{+\infty} (\delta_{n,0} + R_n) S_n = C(1 + e^{2jk_c H}) \quad (6)$$

where

$$S_n = (2b)^{-1} \int_{-b}^b e^{jk_x^{(n)} x} dx = \text{sinc}(k_x^{(n)} b)$$

is the overlap integral between the  $n$ th-order diffracted mode and the fundamental mode inside the cavity, and  $\delta_{n,0}$  is the Kronecker delta function defined as  $\delta_{n,0} = 1$  for  $n = 0$  and  $\delta_{n,0} = 0$  otherwise.

As for the requirement of the continuous particle velocity  $v_y$  at the interface, one may further obtain

$$-\frac{k_y}{\rho_w\omega} e^{jk_x x} + \sum_{n=-\infty}^{+\infty} \frac{k_y^{(n)}}{\rho_w\omega} R_n e^{jk_x^{(n)} x} = \begin{cases} \frac{k_c}{\tilde{\rho}\omega} C(e^{2jk_c H} - 1), & x \in (-b, b) \\ 0, & x \notin (-b, b) \end{cases} \quad (7)$$

Multiplying Eq. (7) by  $e^{-jk_x^{(r)} x}$  ( $r \in \mathbf{Z}$ ) and averaging over the unit-cell area, we have

$$R_r = \delta_{r,0} - C(1 - e^{2jk_c H}) \phi \frac{\rho_w k_c}{\tilde{\rho} k_y^{(r)}} S_r \quad (8)$$

Substituting Eq. (8) into pressure continuity condition (6) yields

$$2S_0 - C(1 - e^{2jk_c H}) \phi^2 \frac{\rho_w}{\tilde{\rho}} \sum_{r=-\infty}^{+\infty} \frac{k_c}{k_y^{(r)}} S_r^2 = C(1 + e^{2jk_c H}) \quad (9)$$

The coefficient  $C$  can be determined from Eq. (9) and is then substituted into Eq. (8). The reflection coefficients of Eq. (9) are determined to be

$$R_n = \delta_{n,0} + \frac{2j \tan(k_c H) \phi (\rho_w / \tilde{\rho}) S_n (k_c / k_y^{(n)})}{1 - j \tan(k_c H) \phi (\rho_w / \tilde{\rho}) \sum_{r=-\infty}^{+\infty} (k_c / k_y^{(r)}) S_r^2} \quad (10)$$

For second-mode instability waves, normal incidence may be hypothesized, i.e.,  $k_x = 0$  and  $k_y = k_0$  [19]. As a result, the formulations of  $v_i$ ,  $p_i$  and  $v_r^{(n)}$ ,  $p_r^{(n)}$  are greatly simplified. Assuming that the periodicity  $s \ll \lambda_{acs}$ , the effective admittance  $A$  can be derived as

$$A = \frac{v}{p} \Big|_{y=0} = \frac{s^{-1} \int_{-s/2}^{s/2} (v_i + \sum_{n=-\infty}^{+\infty} v_r^{(n)})|_{y=0} dx}{s^{-1} \int_{-s/2}^{s/2} (p_i + \sum_{n=-\infty}^{+\infty} p_r^{(n)})|_{y=0} dx} = \frac{\int_{-s/2}^{s/2} \left( -(k_0/\rho_w\omega) + \sum_{n=-\infty}^{+\infty} (\sqrt{k_0^2 - (2\pi n/d)^2} / \rho_w\omega) R_n e^{j(2\pi n/s)x} \right) dx}{\int_{-s/2}^{s/2} \left( 1 + \sum_{n=-\infty}^{+\infty} R_n e^{j(2\pi n/s)x} \right) dx}$$

$$= \frac{(k_0/\rho_w\omega) \int_{-s/2}^{s/2} (R_0 - 1) dx}{\int_{-s/2}^{s/2} (R_0 + 1) dx} = \frac{1}{\rho_w c_w} \frac{R_0 - 1}{R_0 + 1} \quad (11)$$

where the reflection coefficient of the zero-order diffraction (specular refraction) is

$$R_0 = 1 + \frac{2j \tan(k_c H) \phi (\rho_w / \tilde{\rho}) k_c / k_0}{1 - j \tan(k_c H) \phi (\rho_w / \tilde{\rho}) \sum_{r=-\infty}^{+\infty} \frac{k_c}{\sqrt{k_0^2 - (2\pi r / s)^2}} S_r^2} \quad (12)$$

Note that all higher-order diffracted modes are evanescent and cannot radiate to the far field for normal incidence at low frequencies ( $s/\lambda_{acs} \leq 1$ ).

Fedorov's model is first calculated for an isolated deep cavity and then multiplied by porosity  $\phi$  to treat the structured surface as a homogenous surface of uniform effective acoustic admittance [4]. Therefore, the diffracted waves coming from the opening mouth are not considered. To evaluate the overall effect when a plane wave penetrates a porous surface, the present model considers an infinite array of grooves. Because higher-order diffracted modes are included in the derivation, the mutual coupling between disturbances from neighboring cavities is taken into account. In particular, if we neglect all higher-order modes and let the porosity  $\phi$  approach zero (the local oscillation inside each cavity is independent), Eq. (12) reduces to Fedorov's model [12,14]:

$$A = \frac{\phi}{Z_c} j \tan(k_c H) \quad (13)$$

where  $Z_c = \tilde{\rho} \omega / k_c$  is the characteristic impedance inside the cavity.

Figure 2 shows the reflection coefficients of plane monochromatic ultrasonic waves penetrating a porous surface in a quiescent and uniform-temperature atmosphere, with the two aforementioned theoretical models, the numerical results of Brès et al. [14], and by a finite element solver (COMSOL Multiphysics®). The porous parameters are taken from Brès et al. [14], and they are listed as a combination of  $Ar = 0.12$  and  $0.3$  and  $\phi = 0.2, 0.48$ , and  $0.8$ . It should be noted that some of the high-order diffracted modes become propagative, and thus radiate into the propagating mode in free space, when  $s/\lambda_{acs} > 1$  [16]. The specular reflection is obfuscated with high-order diffractions in the upper half-space and cannot be separated from the superposed sound field in our full-wave simulation by COMSOL. Therefore, we do not provide the data when  $f_{acs} > 0.67$ , i.e.,  $s/\lambda_{acs} > 1$  for the case in Fig. 2a. Here,  $f_{acs} =$

$f H / c_w = H / \lambda_{acs}$  is the normalized incidence-wave frequency [14], and  $H/s = \phi / Ar = 0.67$  for the case in Fig. 2a. Also, we would like to emphasize that  $s/\lambda_{acs} = 1$  is a reasonable upper limit of the theoretical model. Actually, the numerical results of Brès et al. [14] were also cut off before  $f_{acs} = 0.67$  for the case in Fig. 2a, but they declared the calculation was strongly affected by the presence of a resonant acoustic mode of frequency  $f_{res} = \phi / Ar$  [20]. In addition, they only showed the results before  $f_{res}/2$  for the case in Fig. 2b, and they attributed the reason to the first subharmonic mode [20]. Nevertheless, the influences of the first subharmonic mode were not observed in other cases. For all cases, the predictions of the proposed model basically coincided with the numerical results from COMSOL and Brès et al. [14], even at high frequency when the wavelength  $\lambda_{acs}$  decreased to the same order of magnitude as  $s$  and the interaction of the scattered waves at the porous surface became strong: for instance, at  $f_{acs} = 0.67$  in Fig. 2a, when the ratio  $s/\lambda_{acs}$  approaches unity. Comparatively, Fedorov's model tends to shift the predicted frequency because it neglects the higher-order diffracted modes. Despite the homogenous hypothesis of  $s \ll \lambda_{acs}$  for both theoretical models, the present model shows the advantage of predicting results that are consistent with numerical results up to the limit  $s/\lambda_{acs} = 1$ . In particular, when  $s/\lambda_{acs} = 1$ , a coupling acoustic mode is reportedly induced by the interaction of waves scattered from adjacent cavities [14,20] and greatly decreases the absorption of the porous coating. This coupling mode is well reproduced by the proposed model, with the predicted  $|R|$  approaching unity. For further illustration, we calculate the distributions of  $|R|$  as a function of porosity  $\phi$  at constant  $Ar = 0.3$ . As shown in Fig. 3, the maximum  $|R|$  appears along the diagonal (dashed line) of the contour plot, where the incident-wave frequency  $f_{acs}$  approaches  $\phi / Ar$ . This observation is exactly the same expression of coupling frequency  $f_{res}$  advocated by Brès et al. based on direct numerical simulation [14,19,20]. Additionally, when the incident-wave frequency is much lower than  $f_{res}$ , both aforementioned theoretical models give results that are consistent with numerical results (Fig. 2d). Moreover, Fig. 3 shows that the minimum  $|R|$  can be achieved by optimizing the cavity-shape parameters. Brès et al. [19] deduced an expression of optimum cavity depth to ensure the phase opposition between the reflection from the solid wall and from the porous surface. However,  $R$  is a nonlinear function of the porosity parameters and flow quantities [Eq. (13)]. A numerical solution seems to be an effective way to obtain the

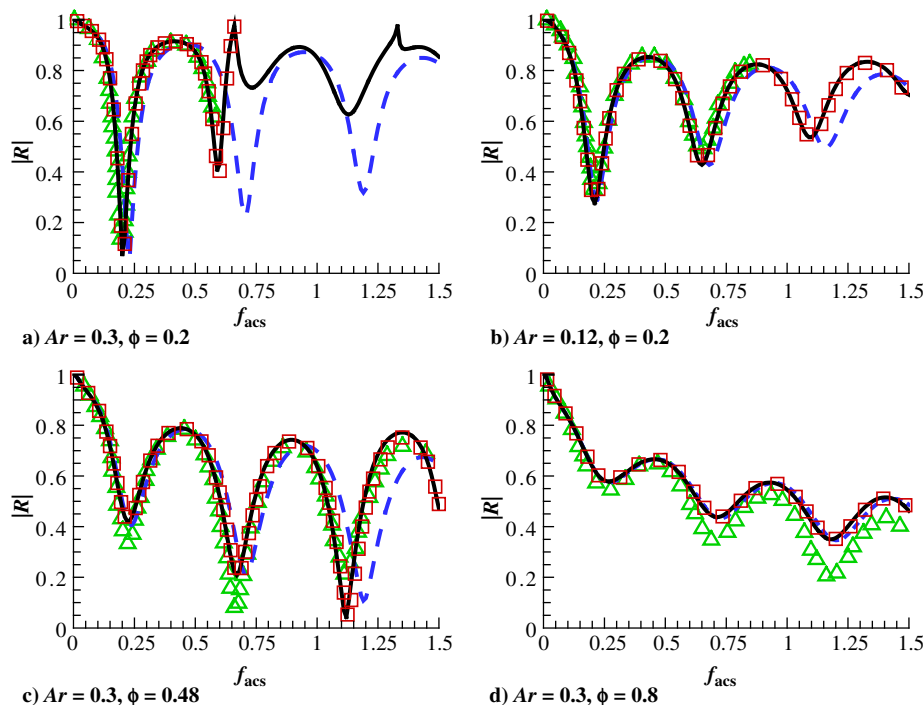


Fig. 2 Reflection coefficient amplitudes obtained from COMSOL (squares), Brès et al. [14] (triangle), Fedorov's model (dashed line), and proposed model (solid line).

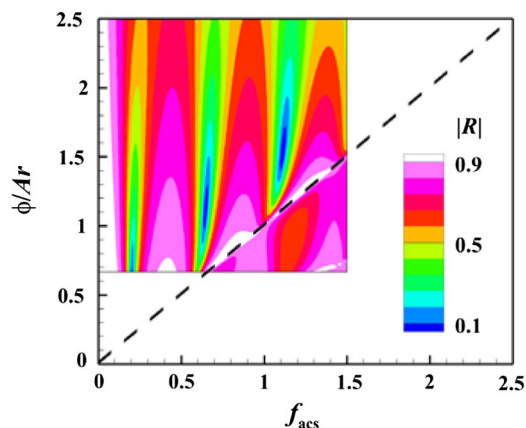


Fig. 3 Contours of reflection coefficient amplitude obtained from proposed theoretical model.

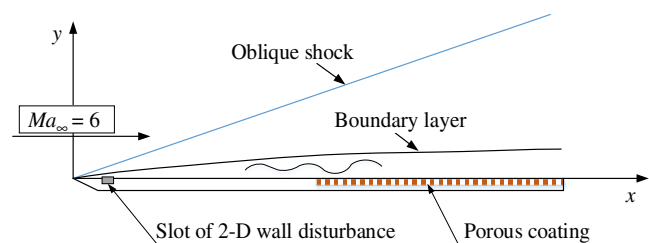


Fig. 4 Schematic drawing of problem formulation. Porous coating is at  $0.5 \leq x/L_{ref} \leq 1.0$ , and  $L_{ref} = 0.2$  m is the reference length.

minimum  $|R|$  by applying triple program loops in the following order: loop 1 is  $0.2 \leq \phi \leq 0.8$ , loop 2 is  $0.06 \leq Ar \leq 0.3$ , and loop 3 is  $0 < f_{acs} < \min(\phi/Ar, 2.0)$ . These parameters span the range of interest for practical applications [14] and ensure the accuracy of the proposed model.

To confirm the proposed optimization strategy, we numerically study the stabilization problem of a hypersonic flow along a two-dimensional (2-D) flat plate at a zero angle of attack (Fig. 4). The freestream flow conditions are the same as in the experiment of Bountin et al. [21]: Mach number  $Ma_\infty = 6.0$ , unit Reynolds number  $Re_\infty = 10.5 \times 10^6 \text{ m}^{-1}$ , and temperature  $T_\infty = 43.18 \text{ K}$ . The wall is isothermal with a temperature of  $T_w = 293 \text{ K}$ . The numerical method and code validation are available in Ref. [22]. An unsteady disturbance is introduced at the beginning of the plate by a slot of periodic suction-blowing at the fixed frequency of 138.74 kHz. The porous coating covers the second half of the plate, and its effect is modeled by the boundary condition  $v'_w = Ap'_w$  at the wall. Because the sound speed  $c_w$  is determined by  $T_w$ , the remaining input flow parameter for Eq. (13) is  $\rho_w$ . In this case, we use the value of  $\rho_w$  at  $x/L_{ref} = 0.75$ , and the optimized shape parameters are  $\phi = 0.66$ ,  $Ar = 0.28$ , and  $f_{acs} = 0.67$ . With these shape parameters, the streamwise minimum  $|R|$  is  $3.4 \times 10^{-5}$  at  $x/L_{ref} = 0.75$ , and the maximum  $|R|$  is  $2.9 \times 10^{-3}$  at  $x/L_{ref} = 0.5$ . For comparison, the performance of a conventional porous coating [14] with relatively deep cavities ( $\phi = 0.66$ ,  $Ar = 0.1$ , and  $f_{acs} = 1.87$ ) is also presented.

Figure 5 shows the instantaneous contours of fluctuating pressure, and Fig. 6 compares the amplitude distributions of fluctuating pressure for the three cases. Here, the fluctuating pressure  $p$  is normalized by  $\rho_\infty u_\infty^2$ , and  $\rho_\infty$  and  $u_\infty$  are the freestream density and velocity, respectively. According to Ref. [22], the Mack second mode dominates along the second half of the plate. Taking the baseline case as an example (Fig. 5a), two-cell structures form downstream ( $x/L_{ref} > 0.5$ ) with a longitudinal wavelength equal to approximately twice the boundary-layer thickness, which corresponds to the typical Mack second-mode structure [23]. Upon installing the porous coating, the Mack second mode is strongly suppressed, especially for the optimized case (Fig. 5b). Notably, upstream of the porous coating,

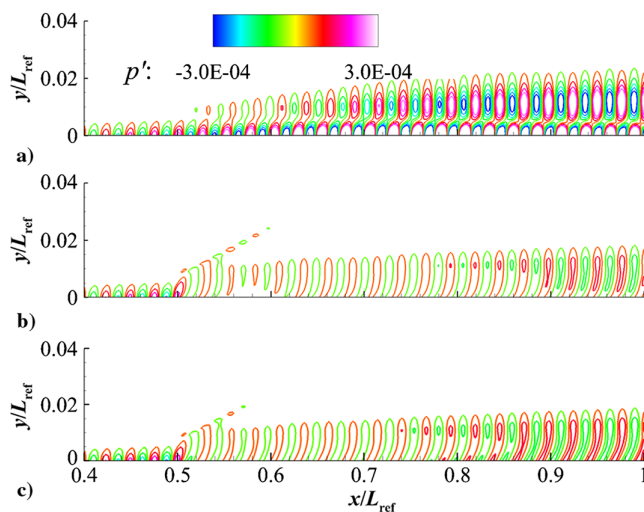


Fig. 5 Instantaneous fluctuating pressure fields for a) baseline case without porous coating, b) optimized one, and c) conventional one.

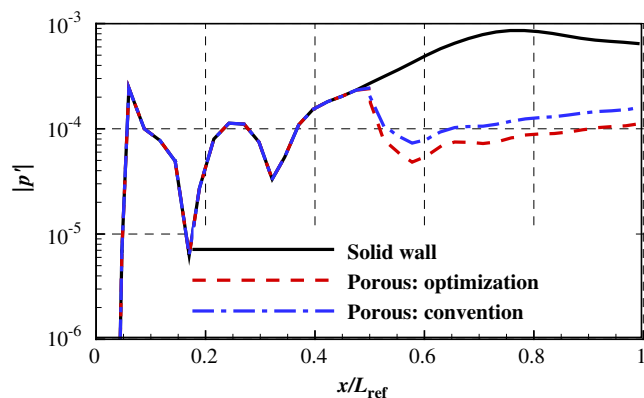


Fig. 6 Amplitude distributions of pressure perturbation along the wall.

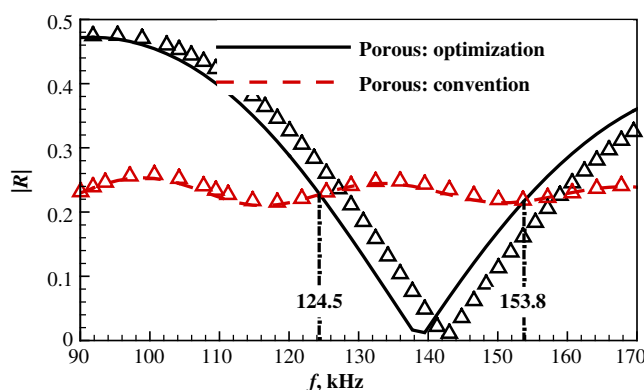


Fig. 7 Calculated reflection coefficients for different disturbance frequencies calculated by the proposed model (line) and Fedorov's model (symbols).

the strong oscillations in Fig. 6 result from the coexistence of multiple waves (including mode  $F$  and mode  $S$  of acoustic waves, and entropy/vorticity waves) in the boundary layer [13,22]. Compared with the baseline case and the conventional porous coating, the maximum fluctuating pressure for the optimized case decreases by 88 and 30%, respectively. Also, the optimized shallow cavity is easier to manufacture. For the second mode wave packets having a frequency band between 88.28 and 176.58 kHz (referred to in Ref. [21]), the

calculated  $|R|$  of the optimized porous coating varies more obviously than those of the conventional one, and its advantage can only be found in a narrow frequency band between 124.5 and 153.8 kHz (Fig. 7). It suggests a porous coating consisting of varied-depth cavities, such as a gradient coating [18], will be a potential candidate to suppress the disturbance with broadband frequencies. Once again, the Fedorov's model shifted the predicted frequency at the optimized shape parameters because it neglects the higher-order diffracted modes (Fig. 7).

### III. Conclusions

In conclusion, an improved theoretical model describing how a porous coating affects the control of the hypersonic boundary-layer transition is proposed herein, taking into account the higher-order diffraction waves generated at the porous surface. Compared with the results of Fedorov's model, the reflection frequency predicted by the proposed model is consistent with numerical data and reproduces the coupling mode between adjacent cavities. Additionally, a straightforward optimization strategy involving program loops is introduced. The Mack second mode is strongly suppressed by the optimized porous coating, with the maximum fluctuating pressure decreasing by about 88%. For the second-mode wave packets having a frequency band, an optimized porous coating with varied-depth cavities will be explored in a future study. This work also indicates that similar theoretical models could be developed to describe porous coatings with pores or cavities of different cross sections.

### Acknowledgments

This study was supported by the Research Grants Council (Hong Kong, under contract no. C5010-14E) and the National Natural Science Foundation of China under grant no. 11402024. We express our honest appreciation to Li Xinliang for his generosity in providing the direct numerical simulation codes.

### References

- [1] Krishnan, K. S. G., Bertram, O., and Seibel, O., "Review of Hybrid Laminar Flow Control Systems," *Progress in Aerospace Science*, Vol. 93, Aug. 2017, pp. 24–52.  
doi:10.1016/j.paerosci.2017.05.005
- [2] Maslov, A. A., "High Speed Boundary Layer Stability and Control," *AIP Conference Proceedings*, Vol. 1376, No. 1, 2011, pp. 18–22.  
doi:10.1063/1.3651827
- [3] Fedorov, A. V., "Prediction and Control of Laminar-Turbulent Transition in High-Speed Boundary-Layer Flows," *Procedia IUTAM*, Vol. 14, 2015, pp. 3–14.  
doi:10.1016/j.piutam.2015.03.017
- [4] Fedorov, A. V., Malmuth, N. D., Rasheed, A., and Hornung, H. G., "Stabilization of Hypersonic Boundary Layers by Porous Coatings," *AIAA Journal*, Vol. 39, No. 4, 2001, pp. 605–610.  
doi:10.2514/2.1382
- [5] Mack, L. M., *Boundary-Layer Stability Theory*, Jet Propulsion Lab., California Inst. of Technology, Pasadena, CA, Nov. 1969.
- [6] Chokani, N., "Nonlinear Evolution of Mack Modes in a Hypersonic Boundary Layer," *Physics of Fluids*, Vol. 17, No. 1, 2005, Paper 014102.  
doi:10.1063/1.1825471
- [7] Fedorov, A., "Transition and Stability of High-Speed Boundary Layers," *Annual Review of Fluid Mechanics*, Vol. 43, No. 1, 2011, pp. 79–95.  
doi:10.1146/annurev-fluid-122109-160750
- [8] Fedorov, A. V., Shiplyuk, A. N., Maslov, A. A., Burov, E., and Malmuth, N. D., "Stabilization of a Hypersonic Boundary Layer Using an Ultrasonically Absorptive Coating," *Journal of Fluid Mechanics*, Vol. 479, March 2003, pp. 99–124.  
doi:10.1017/S0022112002003440
- [9] Sandham, N. D., and Lüdeke, H., "A Numerical Study of Mach 6 Boundary-Layer Stabilization by Means of a Porous Surface," *AIAA Journal*, Vol. 47, No. 9, 2009, pp. 2243–2252.  
doi:10.2514/1.43388
- [10] Wartemann, V., Lüdeke, H., and Sandham, N. D., "Numerical Investigation of Hypersonic Boundary-Layer Stabilization by Porous Surfaces," *AIAA Journal*, Vol. 50, No. 6, 2012, pp. 1281–1290.  
doi:10.2514/1.J051355
- [11] Kirilovskiy, S. V., Poplavskaya, T. V., Tsyryulnikov, I. S., and Maslov, A. A., "Evolution of Disturbances in the Shock Layer on a Flat Plate in the Flow of a Mixture of Vibrationally Excited Gases," *Thermophysics and Aeromechanics*, Vol. 24, No. 3, 2017, pp. 421–430.  
doi:10.1134/S0869864317030106
- [12] Kozlov, V. F., Fedorov, A. V., and Malmuth, N. D., "Acoustic Properties of Rarefied Gases Inside Pores of Simple Geometries," *Journal of the Acoustical Society of America*, Vol. 117, No. 6, 2005, pp. 3402–3411.  
doi:10.1121/1.1893428
- [13] Wang, X., and Zhong, X., "The Stabilization of a Hypersonic Boundary Layer Using Local Sections of Porous Coating," *Physics of Fluids*, Vol. 24, No. 3, 2012, Paper 034105.  
doi:10.1063/1.3694808
- [14] Brès, G. A., Inkmann, M., Colonius, T., and Fedorov, A. V., "Second-Mode Attenuation and Cancellation by Porous Coatings in a High-Speed Boundary Layer," *Journal of Fluid Mechanics*, Vol. 726, July 2013, pp. 312–337.  
doi:10.1017/jfm.2013.206
- [15] Lv, P., Yu, C., Zhang, Y., and Gong, J., "Numerical Investigation of Ultrasonically Absorptive Coating for Hypersonic Laminar Flow Control," *AIAA Paper 2017-2311*, March 2017.
- [16] Wu, T., Cox, T. J., and Lam, Y. W., "From a Profiled Diffuser to an Optimized Absorber," *Journal of the Acoustical Society of America*, Vol. 108, No. 2, 2000, pp. 643–650.  
doi:10.1121/1.429596
- [17] Schwan, L., Geslain, A., Romero-García, V., and Groby, J. P., "Complex Dispersion Relation of Surface Acoustic Waves at a Lossy Metasurface," *Applied Physics Letters*, Vol. 110, No. 5, 2017, Paper 051902.  
doi:10.1063/1.4975120
- [18] Liu, T., Liang, S., Chen, F., and Zhu, J., "Inherent Losses Induced Absorptive Acoustic Rainbow Trapping with a Gradient Metasurface," *Journal of Applied Physics*, Vol. 123, No. 9, 2018, Paper 091702.  
doi:10.1063/1.4997631
- [19] Brès, G. A., Colonius, T., and Fedorov, A. V., "Acoustic Properties of Porous Coatings for Hypersonic Boundary-Layer Control," *AIAA Journal*, Vol. 48, No. 2, 2010, pp. 267–274.  
doi:10.2514/1.40811
- [20] Brès, G. A., Colonius, T., and Fedorov, A. V., "Interaction of Acoustic Disturbances with Micro-Cavities for Ultrasonic Absorptive Coatings," *AIAA Paper 2008-3903*, June 2008.
- [21] Bountin, D., Chimitov, T., Maslov, A., Novikov, A., Egorov, I., Fedorov, A., and Utyuzhnikov, S., "Stabilization of a Hypersonic Boundary Layer Using a Wavy Surface," *AIAA Journal*, Vol. 51, No. 5, 2013, pp. 1203–1210.  
doi:10.2514/1.J052044
- [22] Zhao, R., Wen, C. Y., Tian, X. D., Long, T. H., and Yuan, W., "Numerical Simulation of Local Wall Heating and Cooling Effect on the Stability of a Hypersonic Boundary Layer," *International Journal of Heat and Mass Transfer*, Vol. 121, June 2018, pp. 986–998.
- [23] Egorov, I. V., Fedorov, A. V., and Soudakov, V. G., "Direct Numerical Simulation of Disturbances Generated by Periodic Suction-Blowing in a Hypersonic Boundary Layer," *Theoretical and Computational Fluid Dynamics*, Vol. 20, No. 1, 2006, pp. 41–54.  
doi:10.1007/s00162-005-0001-y

P. Givi  
Associate Editor